Performance Analysis of the Solar Linear Fresnel Reflector

Mohamed H. Ahmed[1]

[1]Solar Energy Dept., National Research Centre, Giza, Egypt

---***--

Abstract - *In recent decades, The Linear Fresnel Reflector (LFR) has attracted considerable attention from the researcher, engineers, and the stakeholders. This attention can be attributed to the characterization of this type of condenser with several advantages that can overcome the problems of other types of solar concentrators. A numerical simulation for the thermal performance of the LFR has been carried out through one year for a certain design under Cairo climate. The effects of the operating parameters (the inlet temperature and flow rate) on the thermal performance of the Solar LFR were investigated. The variation of the incidence angle modifier (IAM) through one year was also studied. The results show an important effect of the daily and seasonal changes in the incidence angle of direct radiation on the IAM and thus thermal performance and concentrator efficiency. At solar noon, the best values for the IAM ranged from 0.9 to 0.98 in June. While the maximum rate of energy gained was about 41 kW and 96 kW for Dec. and June respectively. This numerical model can be used for design optimization to get the maximum efficiency of the solar LRF.*

Key Words: Linear Fresnel Reflector, simulation model, receiver tube, incident angle modifier, concentrator efficiency

1. INTRODUCTION

Solar reflectors are significant tools to concentrate the solar irradiance in a small area to get thermal energy at a high temperature. Despite the widespread deployment and operation of a solar power plant that uses the parabolic trough concentrator (PTC) compare to the Linear Fresnel Reflector (LRC), there are many efforts and attempts to make the LFR a strong competitor in the solar concentrator market. This is because linear Fresnel concentrates have significant technical and economic advantages when compared to the parabolic trough concentrator.

The linear Fresnel concentrators have less thermal efficiency compared to other types of solar concentrators, but the low cost of the LFR may compensate that, providing a solution to the cost problems of solar energy collectors on a large scale [1]. The advantages of Fresnel Linear Concentrations include relatively simple installation and low wind load. It also includes the non-movement of the receiving tube and optimal utilization of available land area [2]. In some stations using Fresnel concentrators, the shaded area under mirrors can be used (e.g. for parking lots) and supply basic needs to rural remote communities. The previous features of the LFR and the low cost of the operation and maintenance (O & m)

results in a significant reduction in the levelized energy cost by about 12 % compared to the parabolic trough concentrator.

The idea on which Fresnel concentrator is based in the use of a series of flat, long and parallel mirrors that focus solar radiation in a linear focus on a receiver tube where the reflected radiation is absorbed by a receiving tube [3] and the non-falling radiation re-reflected again through a secondary compounded parabolic reflector [4]. The outlet temperature and the solar energy to heat energy gained for the linear Fresnel concentrator were investigated at different numbers of mirror elements by Singh et al. [5]. The main drawback of the LFC concentrator is that the concentration ratio is significantly lower than the PTC and changes significantly during the day. However, Muñoz et al. proved that the concentration efficiency achieved by the LRF was very close to the PTC concentration efficiency [6]. Most concentration plants using Fresnel concentrators were used to generate heat at low or medium temperature [7]. For example, small plants that produce thermal energy with temperature ranges from 150 to 300 ºC which are suitable for cooling and heating processes of the buildings [8], domestic heating water [9], steam generation for mining, textile and chemical industries, agriculture and timber and food applications [4]-[10].

The linear Fresnel concentrators differ from each other in terms of reflective mirror width, design of the tracking system and the curvature of the mirror (flat, parabolic, circular), the ratio of the mirror area to the available area, the height of the receiver tube above the primary mirrors, and the details of the receiver: multiple tube receiver or single-tube receiver. Several studies have been conducted on the use of multiple pipes in the receiver tube of the LFC [11], [12]. The multi-pipe receiver tube consists of a group of parallel pipes located inside a cavity and often in the shape of a trapezoid placed in a horizontal plane and thus without a second reflective mirror. Some of the designs for the receiver tube lay a flat glass cover below the cavity to cover the receiver tube and protect the selective surface, which reduces the rate of heat loss. An additional benefit for the glass cover is to make a greenhouse effect that improves the receiver performance. It also minimizes convection losses, due to the vacuum between the steel tube and the glass cover. The main reason for the low of the concentration ratio is the drift and uncertainty in the direction of the reflected radiation with the increase of the length between the mirrors and the receiver.

This article aims to study theoretically the performance of the LFC and the variation of the incident angle modifier through one year. A numerical model was developed using the Engineering Equation Solver (EES) software. The effects of the IAM and the operation parameter on the performance of the LFC were investigated using the simulation program.

2. LFC GEOMETRY

The linear Fresnel concentrator consists of flat or nearly flat mirrors to concentrate the solar radiation on the receiver tube located in the linear focus above the mirror level. The incidence angle θ_i of the sunrays is divided into two angles as shown in Fig. 1. The transversal angle θ_T is defined as the angle between the Zenith and the projection of the direct beam radiation into the transversal plane, while the second angle is the longitudinal angle θ_L and which is the angle between the zenith and the and the projection of the beam radiation into the longitudinal plane [13].
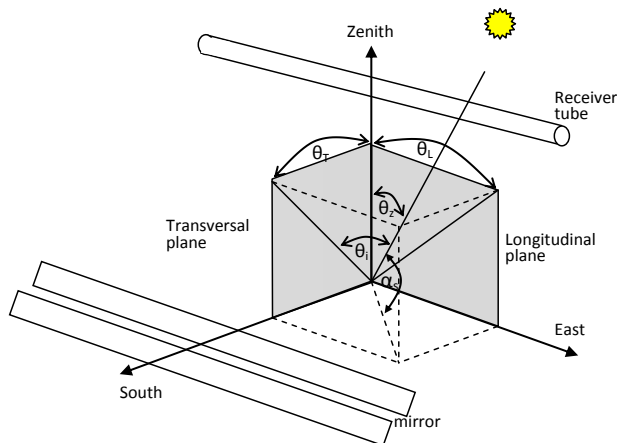

Fig. 1: The important angles of the Linear Fresnel Collector

The net aperture area A_{net} of the LFC collector is the sum of the net aperture area of all mirror rows of the collector and can be calculated as follow:

$$A_{net} = \sum_{i=1}^{n} W_i L \qquad [1]$$

Where W is the aperture width of the mirror row, n is the number of the mirrors and L is the mirror length.

3. The Numerical Model

Using the simulation model, the effect of operating variables such as flow rate and inlet temperature of the heat transfer fluid (HTF) on the thermal performance of the LFR was studied. The study was conducted during the first half of the year and was satisfied due to the similar weather conditions with the second half of the year. The design parameters of the receiver tube and mirrors such as the mirror length and width, curvature of the mirror, the focal length of mirror row, the space between mirror, and the outer and inner diameter

of the receiver tube were included as fixed parameters. The optical parameters of the mirror and receiver tube (transmittance, emittance, absorptance, and Reflectance) were also included in the model as shown in Table I.

The incident solar power $\dot{q}_{input}$ on the receiver tube was calculated from the following equation (According to EN 12975-2):

$$\dot{q}_{input} = A_{net} * DNI * \eta_{otp,p} * IAM(\theta) * ELF \qquad [2]$$

Where the DNI is the direct normal irradiance (w/m²). The maximum optical efficiency $\eta_{opt,p}$ depends on the transmissivity of the glass cover (τ_g), mirror reflectivity (τ_{mi}), and the absorptivity (α_{co}) of the selective surface of the absorber tube.

$$\eta_{otp,p} = \rho_{mi} * \tau_g * \alpha_{co} \qquad [3]$$

The incidence angle modifier IAM (θ_i) can be calculated by multiplying the incidence angle modifier in transversal direction IAMT (θ_T) with the incidence angle modifier in the longitudinal direction IAML (θ_i). Fig. 2 shows the variation of the IAM_T and the IAM_L for different incident angle θ_i.

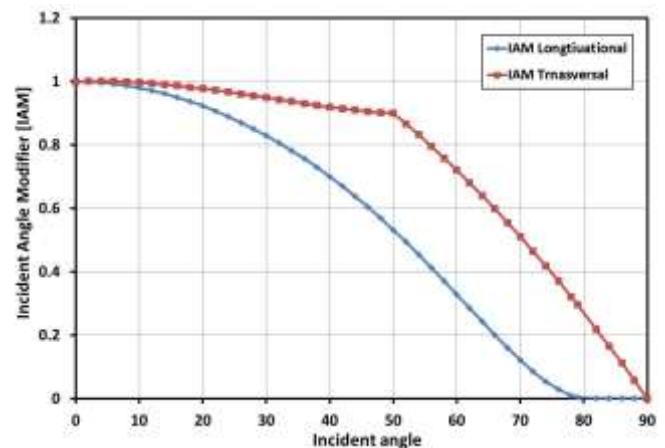$$IAM(\theta) = IAM_L(\theta_i) * IAM_T(\theta_T) \qquad [4]$$

Fig. 2: The incidence angle modifier IAM in longitudinal the and transversal direction

The End Losses Factor (ELF) represent the ratio of the useful receiver length of LFR that receive the concentrated radiation to the total receiver length and it depends on the incidence angle, collector length L and the focal length F and can be expressed as follows:

$$ELF = 1 - \frac{F/\tan\theta_i}{L} \qquad [5]$$

The focal length F can be replaced by an effective focal length F_{eff} for LFR as shown in Fig. 3 [14].
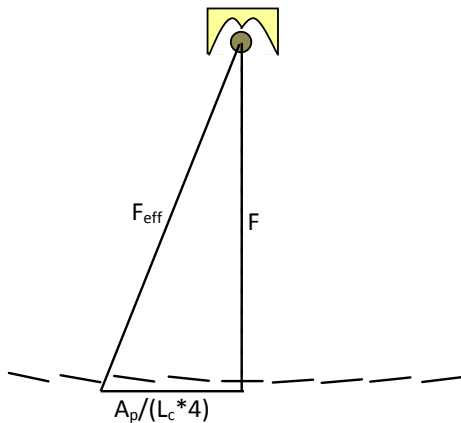
Fig. 3: The effective focal length for the LFC

The receiver unit consists of vacuum receiver tube where the absorber steel tube is located inside a vacuum glass cover and a secondary reflector supported by a second casing and the heat transfer fluid flows inside the absorber tube as illustrated in Fig. 4.
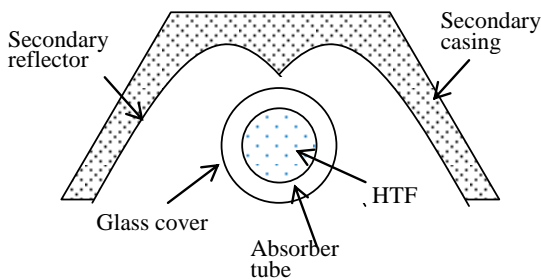

Fig. 4: The construction of the receiver tube assembly

The exit temperature of the HTF, which is synthetic oil, can be calculated by solving the energy balance equations for the absorber tube, glass cover and the HTF in the receiver tube as shown in Fig. 5. The energy equations per unit length for a small segment of length dx for the absorber steel tube, HTF, and the glass cover are as follows:
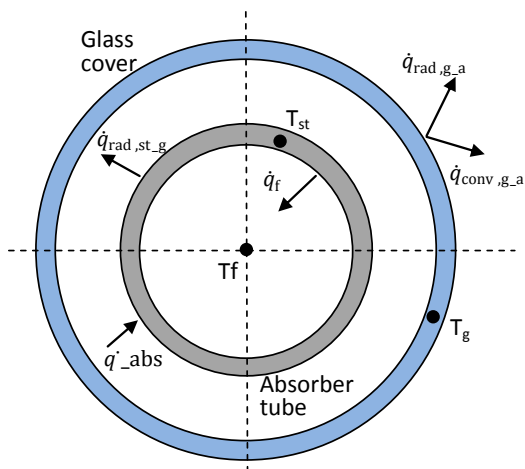

Fig. 5: The energy flow of the receiver tube

The energy balance equation for the heat transfer fluid.

$$h_{c,st-f}\left(T_{s,i} - T_{ms}\right)\pi D_{st,i}dx - q_i + q_o = m_f Cp_f \frac{\partial T_f}{\partial t} \qquad [6]$$

The energy balance equation for the absorber tube

$$\left(q_{abs} - q_{r,st-g}\right)\pi D_{st,o}d - h_{c,st-f}\left(T_{st,i} - T_f\right)$$
$$* \pi D_{st,i}dx = m_{st}Cp_{st}\frac{\partial T_{st}}{\partial t} \qquad [7]$$

The energy balance equation for the glass cover.

$$q_{r,st-g}\pi D_{s,o}dx + q_{abs,g}\pi\left(r_{g,o}^2 - r_{g,i}^2\right)dx$$
$$- \left(q_{c,g-a} + q_{r,g-sky}\right)dx = m_g Cp_g \frac{\partial T_g}{\partial t} \qquad [8]$$

The previous energy balance equations were solved simultaneously using the well-known Engineering Equation Solver (EES) software. The temperature of the absorber steel tube T_{st}, the glass cover temperature T_g, the temperature of the HTF temperature T_f can be calculated. The outlet temperature of the HTF is calculated from the following:

$$T_{out} = 2\,T_f - T_{in} \qquad [9]$$

The output power $\dot{q}_{out}$ transferred from the receiver tube to the heat transfer fluid can be calculated as follows:

$$\dot{q}_{out} = \dot{m}*Cp*(T_{out} - T_{in}) \qquad [10]$$

The rate of the thermal energy losses $\dot{q}_{loss}$ is known as the difference between the rate of input energy to the receiver tube (solar reflected radiation) and the rate of thermal energy gained by the HTF (synthetic oil) $\dot{q}_{out}$.

Some assumptions were taken into consideration to increase the simplicity of the model and analysis. These assumptions were as follows:

▪ The steady state condition was assumed for a small period of the sun movement.

▪ The absorber tube and the glass cover temperature were assumed to be uniform through the small segment.

▪ The temperature variant through the segment thickness of the steel and glass is neglected (one- dimension)

▪ The properties of the steel, glass, and fluid are functioned in their temperature.

▪ The effective focal length was considered for all mirror rows instead of a separate focal length for each row.

▪ The flow inside the absorber tube is fully developed.

Table -1: The parameters used in the simulation program

Design parameter of LFC	value	unit
Inner absorber tube diameter	0.066	m
Outer absorber tube diameter	0.07	m
Mirror width	0.31	m
No. of mirror row	18	
Center focal length	3.564	m
Module length [m]	4	m
No. of module	12	
Internal diameter of glass cover	0.1	m
External diameter glass cover	0.106	m
Receiver coating absorbance	0.958	
Glass cover transmittance	0.964	

4. The Results

The results of the simulation program are presented in this section. The numerical model calculates the incident angle modifier for the LFR though a day based on an experimental data. Fig. 6 presents the incident angle modifier through a complete day in December, March, and June. From the figure, it can be observed that the incident angle increase sharply in the morning and evening period. In December, the maximum incident angle modifier is achieved at 90 min before and after the solar noon and range from 0.46 to 55. While in June, the incident angle modifier reaches its maximum value of about 0.99at exactly solar noon. Stability in the IAM during the day was observed for March.
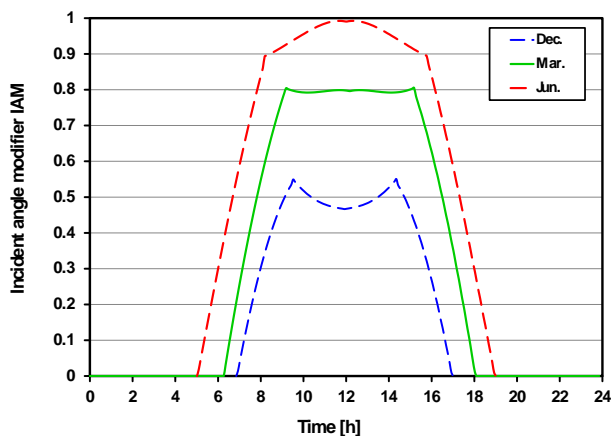

Fig. 6: The incidence angle modifier for the LFR

Fig. 7 presents the temperature of the absorber steel tube and the HTF along the length of the receiver tube of the LFR at different mass flow rates. It can be observed that there is a slight increase in the fluid and steel temperature with the tube length. Increase the flow rate from 1 to 1.6 kg/s leads to a decrease in the outlet fluid temperature from 150.5 to 132 ºC, respectively.
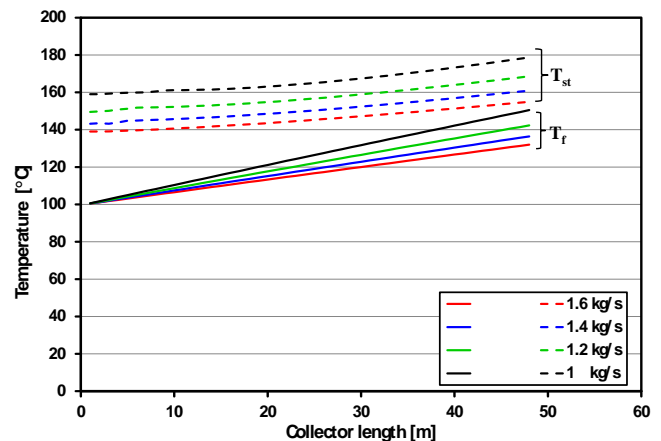

Fig. 7: The effect of the mass flow rate on the steel tube and fluid temperature

There is an unnoticeable effect of the mass flow rate on the fluid temperature at the first part of the receiver tube length while this effect becomes noticeable gradually with the progression of the fluid through the receiver tube length.

Fig. 8 presents the daily variation of the HTF temperature rise ΔT during six months of the year. The temperature rise reaches its maximum value at solar noon where it ranges from 20 to 42 ºC from January to June, respectively.
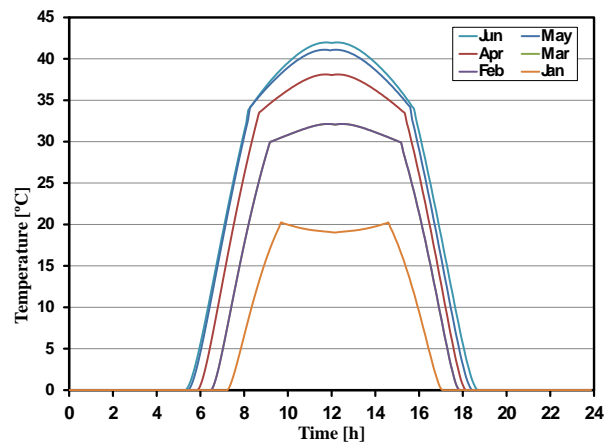

Fig. 8: The temperature rise of the HTF at different months.

The rate of thermal energy gained through a year changes from month to other where it affected by the incident angle modifier IAM. Fig. 9 present the thermal energy gained for December, March, and June. The rate of energy gained takes the same trend as the temperature rise where it reaches a maximum value of about 69.9 and 95.5 kW at solar noon in March and June, respectively. While for December, there are two maximum values at 90 min before and after the solar noon. That can be attributed to the profile of the incidence angle and the IAM during the day of these months.
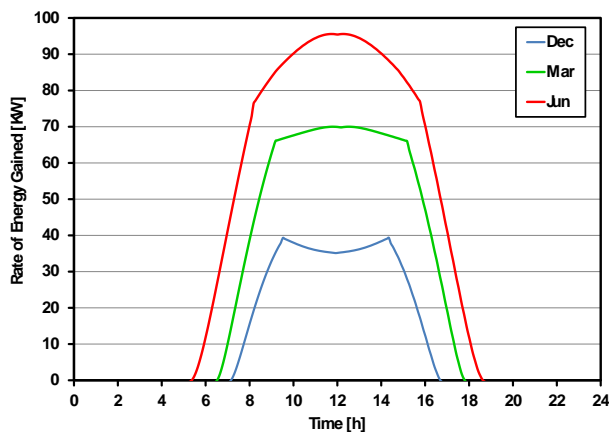
Fig. 9: The rate of energy gained from the LFR for December, March, and June months

It can be observed also a sharp increase and decrease in the rate of energy gained in the early morning and late evening. In the noon period, different changes in the rate of energy gained by about 20, 5 and 10% were observed for June, March, and December, respectively. From the previous, it can be concluded that the rate of output energy from the LFR is more stable in the spring and autumn months but it has significant variations during the summer months.

The effects of the inlet temperature of the HTF on the temperature rise through the LFC are shown in Fig. 10. From the figure, it can be observed that increasing the inlet temperature from 80 to 200 °C leads to a decrease in the temperature rise by about 12 % for all ranges of mass flow rate. While increasing the flow rate from 0.9 to 1.3 kg/s leads to a decreasing in the temperature rise by about 30 %.
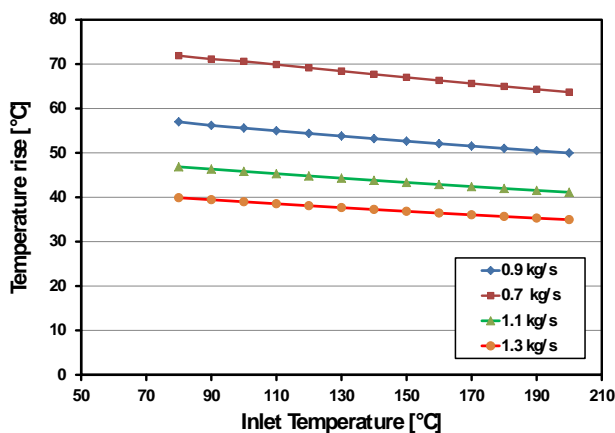

Fig. 10: Effect of the inlet temperature on the oil temperature rise

The effect of the inlet temperature on the LFR efficiency is presented at different mass flow rates in Fig. 11. From the figure, it can be noticed that a slight increase in the efficiency from 47.7 to 48.3 % was recorded during increasing the mass flow rate from 0.7 to 1.3 kg/s at all inlet temperatures. Increasing the inlet temperature leads to a slight decrease in

the LFR efficiency for all mass flow rate where the efficiency decrease from 48.5 to 47.5 %with increasing the inlet temperature from 80 to 200 ºC, respectively.
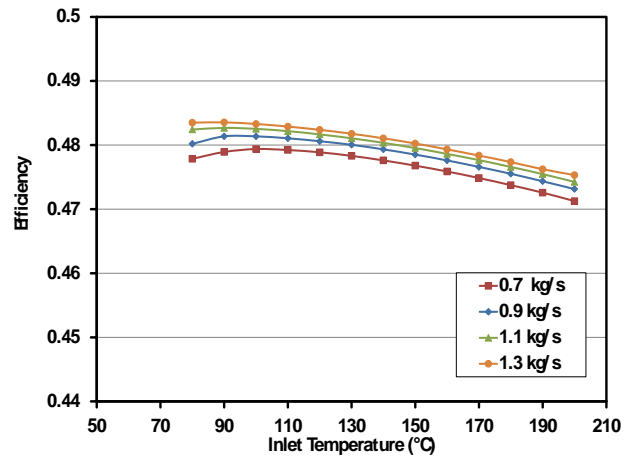

Fig. 11: Effect of the inlet temperature on the LFR efficiency

4. CONCLUSIONS

From the previous results, it can be concluded that the effect of the incidence angle has a significant role in the incidence angle modifier and the incident radiation on the receiver tube. The IAM is at its highest value ranging from 0.9 to 0.99 around solar noon in Jun and at its lowest value ranging from 0.46 to 0.55 in December. At solar noon, the temperature rise ranges from 20 to 42 °C for December and Jun, respectively. The other conclusion from the theoretical study is that the rate of energy gained is very small at the early morning and late evening and increase sharply to reach a maximum value of about 41 kW around the solar noon in winter. But in the summer, the rate of energy gained reaches a maximum value of about 96 kW. The effect of inlet fluid temperature on the temperature rise and collector efficiency is smaller compared to the effect of the fluid mass flow rate.

Nomenclature

A:	Area (m²)
Cp:	Specific heat
D:	Diameter (m)
F:	Focal length (m)
L:	Mirror length (m²)
m:	mass (kg)
h:	heat transfer coefficient (W/m² °C)
$\dot{m}$:	Mass flow rate (kg/s)
$\dot{q}$:	Rate of energy (W)
T:	Temperature (°C)
t:	Time (s)
W:	Mirror width (m²)
θ:	Incidence angle
η:	Efficiency
ρ:	Reflectivity

τ: Transmissivity
α: Absorptivity

Subscripts

a: Ambient
abs: absorbed
i: Inside
o: Outside
in: Inlet
out: Outlet
c: Heat transfer by convection
st   Steel tube
f: Fluid
g: Glass
r: Heat transfer by radiation

ACKNOWLEDGEMENT

REFERENCES

[1]   D. Buie, C. Dey, and D. Mills, "Optical considerations in line focus Fresnel concentrators," in Proc. of 11th International SolarPaces Conference, Zurich, Switzerland, 2002.

[2]   A. Häberle, et al., "Linear concentrating Fresnel collector for process heat applications," in Proc. of 13th International Symposium on Concentrated Solar Power and Chemical Energy Technologies, Sevilla, Spain, 2006.

[3]   D. R. Mills and G. L. Morrison, "Compact linear fresnel reflector solar thermal power plants," Solar Energy, vol. 68, No. 3, Mar. 2000, pp. 263-283, doi.org/10.1016/S0038-092X(99)00068-7.

[4]   G. Morin, M. Mertins, J. Kirchberger, and M. Selig, "Supernova construction, control & performance of steam superheating linear fresnel collector," in Proc. of SolarPaces International Symposium, 2011, pp. 1-6.

[5]   P. L. Singh, S. Ganesan, and G. C. Yadav, "Performance study of a linear fresnel concentrating solar device," Renewable Energy Focus, vol. 18, Nov. 1999, pp. 409-416, doi.org/10.1016/S0960-1481(98)00805-2.

[6]   J. Muñoz, J. M. Martı́nez-Val, and A. Ramos, "Thermal regimes in solar-thermal linear collectors," Solar Energy, vol. 85, No. 5, May 2011, pp. 857-870, doi.org/10.1016/j.solener.2011.02.004.

[7]   G. Zhu, "Development of an analytical optical method for linear Fresnel collectors," Solar Energy, vol. 94, Aug. 2013, pp. 240-252, doi.org/10.1016/j.solener.2013.05.003.

[8]   P. Bermejo, F. J. Pino, and F. Rosa, "Solar absorption cooling plant in Seville," Solar Energy, vol. 84, No. 8, Aug. 2010, pp. 1503-1512, doi.org/10.1016/j.solener.2010.05.012.

[9]   T. Sultana, G. L. Morrison, and G. Rosengarten, "Thermal performance of a novel rooftop solar micro-concentrating collector," Solar Energy, vol. 86, no. 7, Jul. 2012, pp. 1992-2000, doi.org/10.1016/j.solener.2012.04.002.

[10] J. Rawlins and M. Ashcroft. Small scale concentrated solar power–A review of current activity and potential to accelerate employment –Report. carbon trust 2013. [Online]:https://www.gov.uk/government/uploads/system /uploads/attachment_data/file/191058/

[11] G. Francia, "Pilots plants of solar steam generating stations," Solar Energy, vol. 12, Sept. 1968, pp. 51-64,. doi.org/10.1016/0038-092X(68)90024-8.

[12] G. Di Canio, W. J. Treytl, F. A. Jur, and C. D. Watson, "Line focus solar thermal central receiver research study-final report," Prepared for the US Department of Energy by FMC Corporation, Santa Clara, CA, 1979.

[13] M. Mertins, "Technical and economic analysis of horizontal Fresnel collectors," Ph.D. thesis, Karlsruhe University, Germany, 2009.

[14] A. Heimsath, G. Bern, D. van Rooyen and P. Nitz, "Quantifying optical loss factors of small linear concentrating collectors for process heat application," Energy Procedia, vol. 48, 2014, pp. 77-86, doi.org/10.1016/j.egypro.2014.02.010.